

---

---

# Spectral and Radiometric Calibration of the Advanced Land Imager

Jeffrey A. Mendenhall, Donald E. Lencioni, and Jenifer B. Evans

■ The Advanced Land Imager (ALI) is currently flying aboard the Earth Observing 1 (EO-1) mission under NASA's New Millennium Program. Initial ground calibration and on-orbit calibration procedures for the ALI were established to ensure accurate spectral and radiometric measurements. Periodic recertification is performed with solar, lunar, and onboard lamp sources. As a result of the on-orbit data stability and drift, several mechanical steps, including temperature cycling, have been implemented.

CALIBRATION OF SPECTRAL AND RADIOMETRIC measurements of the Advanced Land Imager (ALI) is a critical element of its land-sensing mission. Without initial ground-based and subsequent on-orbit standardization, the data cannot be reliably used for the intricate analysis of atmospheric conditions and complex surface regions. Daily, weekly, and monthly recertification steps are taken to recalibrate the instrument for any spectral or radiometric fluctuations or drift.

Ground calibration of the ALI occurred from September 1998 through January 1999 at Lincoln Laboratory [1–4]. In this article, we outline the techniques adopted during the ground-based spectral and radiometric calibration of the ALI and present results derived from subsystem- and system-level measurements. Results from on-orbit calibration and testing are also presented and compared with the ground-based data.

## Focal-Plane Construction

The focal plane of the ALI contains silicon and non-cryogenic mercury-cadmium-telluride (HgCdTe) multispectral and panchromatic detector arrays with a total of ten spectral bands spanning the 400 to 2500 nm wavelength region [5–9]. Table 1 lists these spec-

tral bands by wavelength and ground sample distance. These bands have been designed to mimic five Landsat [10] spectral bands and provide two additional bands covering wavelengths from 433 to 453 nm and from 1200 to 1300 nm. Furthermore, the region covered by Landsat band 4 has been divided into two separate bands (4, 4p) in order to avoid a water-vapor line at 825 nm. The partially populated focal plane provides a 3° cross-track coverage corresponding to 37 km on the ground. The focal-plane temperature is maintained at 220 K by means of a passive radiator.

Although the ALI optical system supports a 15° wide field of view, only 3° of the focal plane was populated with detector arrays. Four sensor chip assemblies (SCA) populate the 3° cross-track segment to form the active focal-plane array (FPA). Each multispectral band on each SCA contains 320 detectors in the cross-track direction, while each panchromatic band contains 960 detectors.

The multispectral/panchromatic arrays use silicon-diode visible and near infrared (VNIR) detectors fabricated on the silicon substrate of a read-out integrated circuit (ROIC). The shortwave infrared (SWIR) detectors are HgCdTe photodiodes that are indium bump-bonded onto the ROIC that services the VNIR

**Table 1. Spectral and Spatial Definitions for the Ten ALI Bands**

Band*	Wavelength (nm)	Ground sampling distance (m)
Panchromatic	480–690	10
1p	433–453	30
1	450–515	30
2	525–605	30
3	633–690	30
4	775–805	30
4p	845–890	30
5p	1200–1300	30
5	1550–1750	30
7	2080–2350	30

\* Bands 1 through 4p are visible and near infrared (VNIR) detectors, while bands 5p, 5, and 7 are shortwave infrared (SWIR) detectors.

detectors. These SWIR detectors promise high performance over the 900 to 2500 nm wavelength region at temperatures that can be reached by passive or thermoelectric cooling. The nominal focal-plane tempera-

ture is 220K and is maintained by the use of a radiator and heater controls.

The spectral bands for each multispectral channel are defined by filters lying above the silicon and HgCdTe detectors. Figure 1 shows a cross-sectional view of an individual SCA. A three-piece sandwich design is used to construct the filters for bands 1p, 1, 2, and the panchromatic band. All other band filters use a single glass design. We cemented all glass segments together with Epotek 301 and the ten filters together form an assembly that resides in a bezel mounted directly above the detector arrays.

### Spectral Calibration

The spectral response of the ALI is defined by mirror reflectivity and focal-plane filter transmissions and detector responsivities. Spectral calibration of the ALI was conducted on both the subsystem and the system level.

#### Subsystem-Level Spectral Response Measurement Techniques

The predicted system-level spectral response for each band has been calculated analytically as the product of the spectral responses of individual ALI optical components. Component-level spectral characterizations

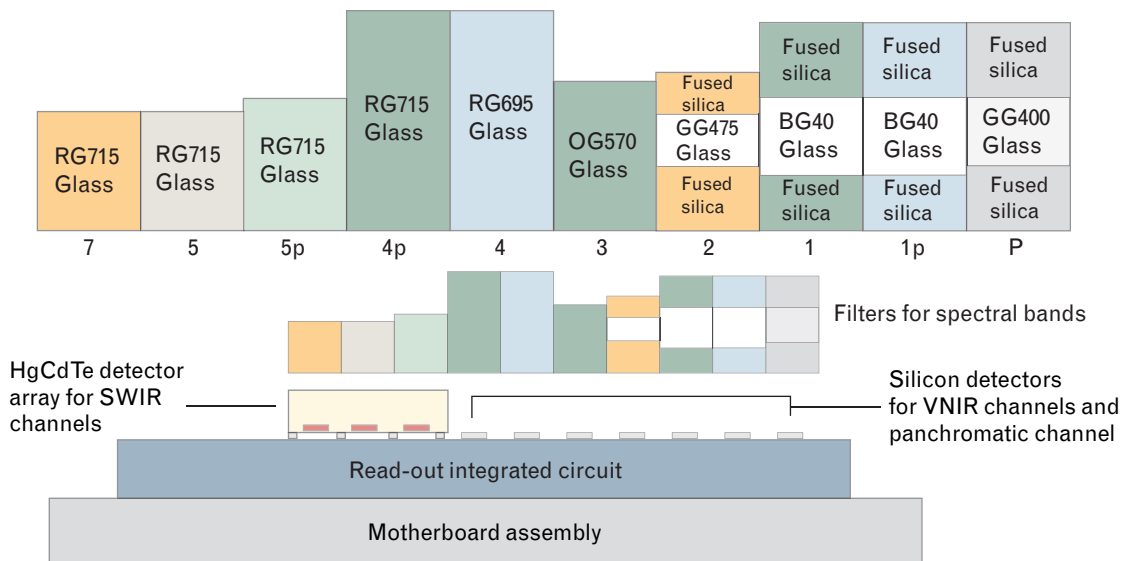


**FIGURE 1.** Focal-plane-array cross-section of a sensor chip assembly (SCA). The panchromatic band (P) and bands 1p through 4p are silicon-diode visible and near infrared (VNIR) detectors mounted directly on the silicon substrate. Bands 5p, 5, and 7 are shortwave infrared (SWIR) detectors.

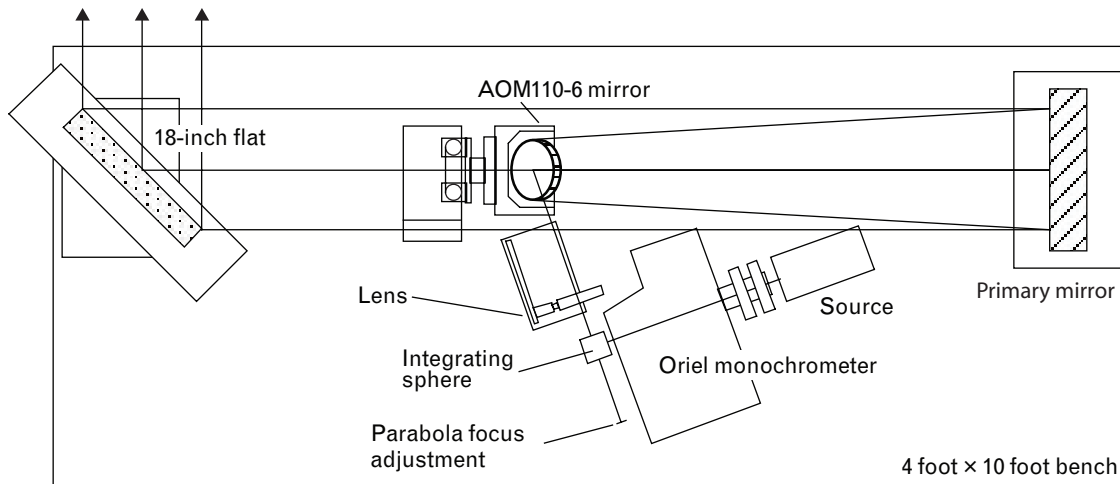


**FIGURE 2.** Spectral collimator used during spectral calibration of the Advanced Land Imager (ALI). The source is calibrated to a NIST traceable source, and is then used to calibrate the integrating sphere. The lens is a Melles Griot 01 LPX245 with a focal length of 15 mm and a diameter of 105 mm. The primary mirror is a 2.54 m (100 in) off-axis parabolic mirror.

include measurements of witness sample detector responsivities by the Santa Barbara Research Center (now the Raytheon Infrared Center of Excellence), filter transmissions by Barr Associates, and mirrors one through three (M1, M2, and M3) and the flat folding mirror (M4) reflectivities by SSG Incorporated.

*Subsystem-Level Analysis.* The generation of system-level spectral response functions based on component-level measurements must account for all elements that affect the response of an assembled instrument: mirror reflectivities, filter transmissions, and detector responsivities. Reduced witness sample data for each of these components were provided by each manufacturer as a part of Lincoln Laboratory quality control during instrument construction. Five VNIR and sixty SWIR detector responsivity measurements, 20 nm interval mirror reflectivity measurements, and 0.5 and 1 nm interval filter transmission measurements were used in this analysis. Each of these data sets was interpolated onto a 1 nm spectral sampling interval. The overall system-level performance was calculated for each band as the product of component measurements as a function of wavelength, normalized to unity at the peak response.

#### *System-Level Spectral Response Measurement Techniques*

System-level spectral calibration of the fully assembled flight instrument was performed at Lincoln Labora-

tory under vacuum at expected flight temperatures. A spectral collimator was used to project a monochromatic beam into the vacuum tank via a quartz window. Data were collected from 400 nm to 2500 nm to map both in-band and out-of-band response for pixels in each of the multispectral and panchromatic bands.

Figure 2 illustrates the three sections of the spectral collimator used during system-level spectral characterization of the ALI: source, collimating optics, and beam monitor. The source was composed of a quartz-tungsten halogen lamp assembly, monochromator, integrating sphere, and condensing lens. The halogen lamp assembly provided a stable broadband source and was used to fill the  $f/4$  entrance cone of the monochromator. The wavelength and spectral bandwidth passing through the system were defined by the order-sorting filters, diffraction gratings, and slit widths of the Oriel MS257 monochromator. Upon exiting the monochromator, the beam was randomized into a uniform 1.27 cm (0.5 inch) diameter spot by using a 5.08 cm (2 inch) inner diameter Labsphere Spectralon integrating sphere. A condensing lens (01 LPX 245) was positioned to expand the output of the integrating sphere and provide a 7.62 cm (3 inch) diameter field for calibration.

The primary component of the spectral collimating optics was a 43.8 cm (17 inch) diameter, 2.54 m (100 inch) focal-length off-axis parabola. This mirror was

mounted such that its focus was collocated with the virtual image of the integrating sphere output formed by the condensing lens. Collimated radiation reflected from the parabola was directed into the vacuum-tank window by using a large 45.72 cm (18 inch) diameter flat folding mirror. A light tent was positioned around the spectral collimator and an intricate baffling scheme was adopted to prevent stray light from contaminating the dim monochromatic output for this measurement.

The collimator contained two reference detectors, which were used to monitor the beam stability and flux throughout spectral calibration of the instrument. It also contained a silicon detector for VNIR measurements and a lead sulfide detector for SWIR measurements. Each detector, located between the 18-inch flat folding mirror and the vacuum-tank window, was chopped and a lock-in amplifier was used to accurately subtract dark-current drift and background radiation.

System-level spectral calibration data were collected in December 1998 and January 1999 in a class 1000 clean room at Lincoln Laboratory. This calibration was conducted with the ALI as a fully assembled instrument in a thermal-vacuum chamber at operational temperatures.

A Dell 266 MHz PC (Windows 95 platform) controlled the monochromator scanning and beam sampling by using a general-purpose interface bus (GPIB) interface and LabView control software. For VNIR measurements (400 to 1000 nm) a spectral bandwidth and sampling interval of 2 nm was used. For SWIR measurements (1000 to 2500 nm) a spectral bandwidth and sampling interval of 4 nm was used.

Data collection consisted of iteratively sampling the beam with the reference detector and the ALI at each wavelength interval. Initially, a wavelength and bandpass were set by the monochromator. A translation stage then positioned the silicon or lead sulfide detector and chopper between the 18-inch flat folding mirror and vacuum-tank window. After sampling the beam, the detector was moved to an out-of-beam position. All bands of the ALI then sampled the monochromatic beam. Finally, a filter wheel, acting as a shutter between the light source and monochromator, blocked the incident beam to provide a dark ALI reference for each spectral sample.

*System-Level Analysis.* Analysis of the ALI system-level spectral calibration data was centered on the normalization of a given pixel's response (digital number, or  $dn$ ) to account for beam-intensity and vacuum-tank-window transmission artifacts as a function of wavelength ( $\lambda$ ). Initially, the ALI pixel response was offset-corrected by subtracting dark-scene values for each wavelength. A plot of spectral transmission versus wavelength was then generated for a given pixel by accessing data for a particular spectral calibration run and the wavelengths covered at that time. Artifacts induced by the vacuum-tank window were then removed by dividing the pixel's spectral response by the window's previously measured spectral transmission.

Next, the varying intensity of the incident beam as a function of wavelength was accounted for by dividing the pixel spectral response by the beam intensity measured at each wavelength by the silicon or lead sulfide detectors. Finally, the spectral response of the reference detector itself was removed by dividing the beam intensity measurement by the detector's responsivity for the spectral range of interest. The above technique is shown analytically by the following relation:

$$S_p(\lambda) = \frac{A_p(dn, \lambda)R_d(\lambda)}{T_w(\lambda)F(\lambda)}. \quad (1)$$

Here,  $S_p(\lambda)$  is the derived spectral response for pixel  $P$  as a function of wavelength  $\lambda$ ,  $A_p(dn, \lambda)$  is the ALI focal-plane response for pixel  $P$  as a function of digital number  $dn$  and wavelength  $\lambda$ ,  $T_w(\lambda)$  is the spectral transmission of the vacuum-tank window, and  $F(\lambda)$  is the measured reference detector response to the beam as function of wavelength.  $R_d(\lambda)$  is the spectral responsivity of the detector used to measure the beam.

Once the above corrections are applied, the resulting spectral response function for a given pixel is normalized to unity at the peak response. Responses for 200 pixels are then averaged and compared to the theoretical spectral response of the ALI (generated from the component measurements).

### Results

We have measured the system-level spectral response function for each ALI VNIR, SWIR, and panchromatic band. We find excellent morphological agree-

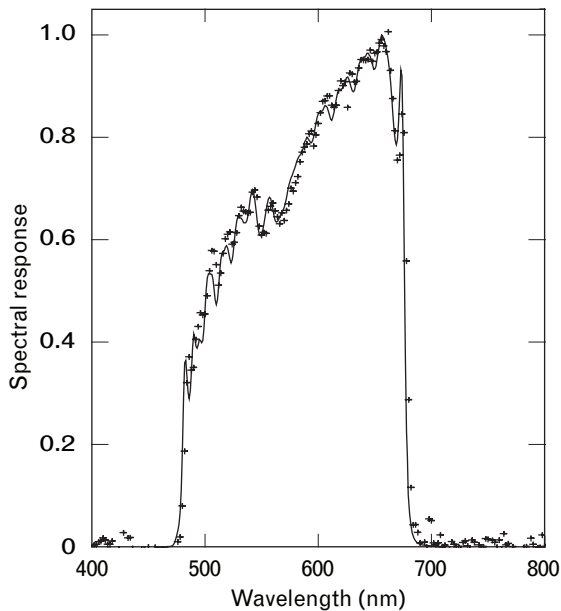


**FIGURE 3.** Spectral response of the panchromatic band. The crosses represent the mean system-level measured response for 200 pixels. The solid line represents data collected during subsystem-level measurements.

ment (<5% near peak transmissions) for all bands. Figure 3 shows the spectral response of the panchromatic band, which demonstrates good agreement between system- and component-level measurements despite intricate variability across this band's spectral bandpass. By using fitting programs for spectral analysis, we also find that the cut-on and cut-off wavelengths agree with subsystem-level measurements to within 1 nm for VNIR bands and 2 nm for SWIR bands. Finally, component-level measurements demonstrate out-of-band responses less than 0.03% for all bands. System-

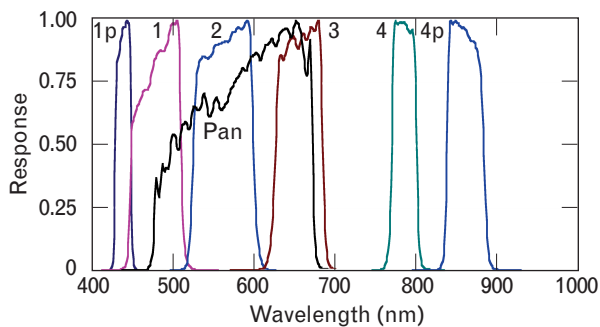


**FIGURE 4.** Normalized visible and near infrared (VNIR) spectral response functions based on subsystem-level measurements.

level measurements revealed no out-of-band response for all bands down to the noise level of the ALI.

### Summary

We find the system-level ALI VNIR, SWIR and panchromatic spectral response measurements are in excellent agreement with theoretical models generated from component measurements. We find the spectral response of the ALI to be primarily dependent on the spectral response of the band-defining filters lying directly above the focal plane. Detector responsivities have a smaller effect on the spectral response of this instrument. This is particularly true for bands with larger bandpasses, such as the panchromatic band. For this band, the gradually increasing efficiency of the silicon material must be accounted for to accurately predict the spectral response of the ALI. Finally, mirror response has little effect on the spectral response of the instrument above 500 nm, providing a global diminution of approximately 5%, which is not a factor when band responses are normalized to unity. However, mirror reflectivities do fall off (down to 80%) below 500 nm and so must be properly accounted for when we consider bands in this spectral range.

We have adopted response functions based on the finer spectrally sampled component measurements as the spectral response of the ALI for the VNIR, SWIR, and panchromatic bands. These responses, illustrated in Figures 4 and 5, define the spectral bandpass for each band during the analysis of in-flight data. These responses have also been adopted for calculating the in-band radiance of each pixel during radiometric calibration of the ALI [1].

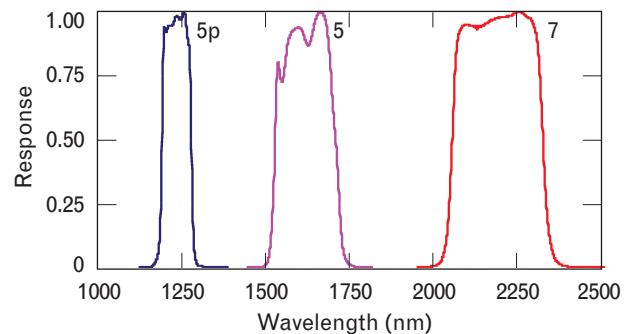


**FIGURE 5.** Normalized shortwave infrared (SWIR) spectral response functions based on subsystem-level measurements.

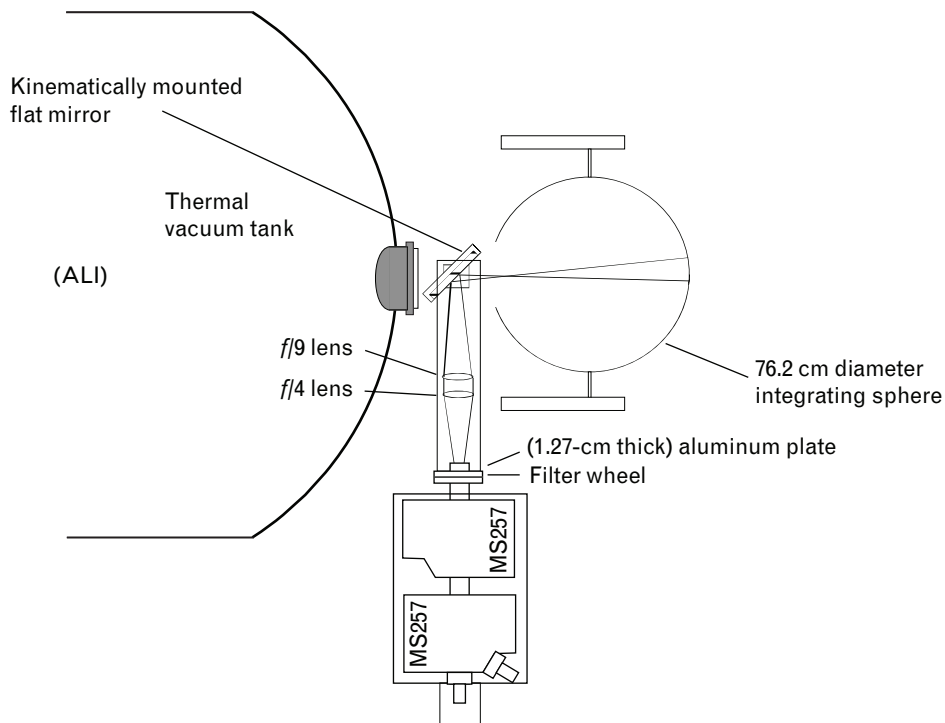


**FIGURE 6.** Integrating sphere and spectro-radiometer used during radiometric calibration of the ALI.

### Preflight Radiometric Calibration

The radiometric response of the ALI was first measured at the system level during ground calibration activities at Lincoln Laboratory in the fall of 1998 [1–4]. Characterization of the radiometric performance of the instrument included measurement of the instrument’s absolute response, signal-to-noise ratio, saturation radiance, and dynamic range. Verification and monitoring of the instrument’s response was then performed by using a variety of techniques once the ALI was on-orbit.

The technique that was adopted for the measurement of the radiometric response of each ALI detector consisted of flooding the instrument entrance aperture with a diffuse source of stable broadband emission. The source of diffuse emission is a 76.2 cm diameter integrating sphere with a 25.4 cm diameter output port manufactured by Labsphere Inc. Figure 6 illustrates the relative configuration of this sphere with the other components of the spectro-radiometer. The sphere contains three internally mounted 150 watt and one externally mounted 125 watt halogen lamps.

These lamps provide a combined radiance equal to 100% earth-equivalent albedo for bands 3, 4, 4p, 5p, 5, and 7 and the panchromatic band. Four additional externally mounted 300W xenon lamps were also used to provide 100% earth-equivalent albedo for bands 1p, 1, and 2. Additional radiance levels were obtained through a combination of sequentially extinguishing lamps, de-rating one internal-reference-amp current, and exercising a GPIB-controlled linear attenuator mounted between the external halogen source and the integrating sphere. A similar attenuator was also located between one of the externally mounted xenon sources and the sphere to provide more flexibility in selecting radiance levels for bands 1p, 1, and 2.

### NIST Traceability

A radiometric-transfer-standard system, shown in Figures 6 and 7, was constructed at Lincoln Laboratory to provide absolute radiometric traceability to other sensors. The principal components of the system are an irradiance source, traceable to the National Institute of Standards and Technology (NIST), and an Oriel MS257 monochromator used as a spectro-radi-

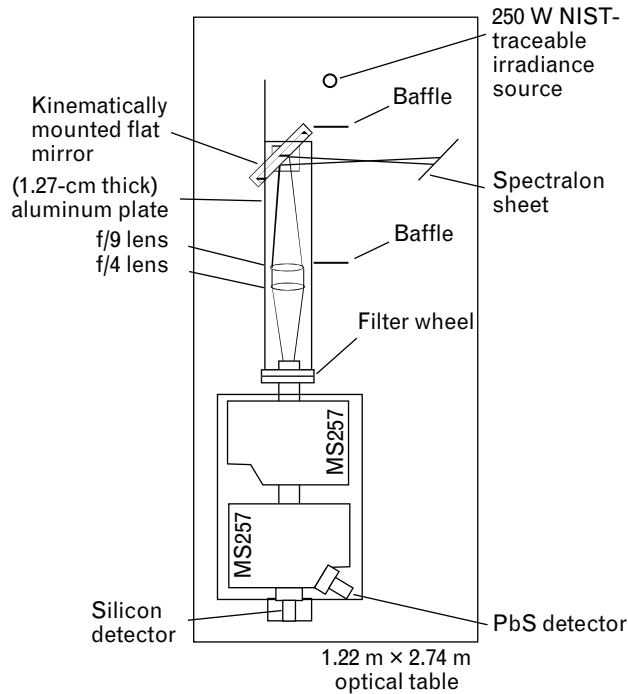


**FIGURE 7.** Radiometric-transfer-standard system built at Lincoln Laboratory. The NIST-traceable source calibrates the Spectralon sheet and the spectrometers, which in turn calibrate the integrating sphere. The integrating sphere is used as one of the on-orbit calibrations.

ometer. The 250 watt irradiance source was mounted on a post with proper baffling to control stray light from the room and reflections from the source off other surfaces. A calibrated radiance scene was generated by placing a Labsphere Spectralon sheet 50 cm from the irradiance source. The monochromator field of view was limited to a  $6.45 \text{ cm}^2$  (1 square inch) region of the diffuse scene to maintain the traceability of the radiance source. A 15.24 cm flat folding mirror was placed between the Spectralon diffuser and entrance slit of the monochromator for convenient location of the source.

By alternately scanning the radiance scene produced by the standard lamp and various radiance levels output by the large integrating sphere, we established radiometric NIST traceabil-

ity for the ALI. Additional near real-time monitoring of the sphere radiance level was accomplished by mounting the flat folding mirror on a post between the vacuum-tank window and the integrating sphere. During radiometric calibration of the ALI, the mirror was removed and the response of the focal plane was recorded. Between ALI data collections, the mirror was kinematically mounted on the aluminum bar, redirecting a portion of the sphere radiance into the entrance slit of the spectro-radiometer. The radiance of the integrating sphere was then measured from 300 to 2500 nm in 10 nm intervals with 5 nm full-width-half-maximum resolution. Finally, silicon and germanium detectors, mechanically mounted to the sphere wall, provided continuous broadband monitoring of the sphere stability.

Table 2 provides a listing of contributing errors to the radiometric calibration technique at three wavelengths. The dominant factor in the VNIR spectral range is the NIST standard lamp. Near 1300 nm the repeatability of the lead sulfide spectro-radiometer detector dominates the uncertainty in the measurement, followed closely by the standard lamp. Finally, at 2000 nm, the standard lamp provides the largest degree of uncertainty in the measurement.

**Table 2. Radiometric Calibration Error Budget**

Source	$1\sigma$ error (%)		
	600 nm	1300 nm	2000 nm
NIST standard lamp	0.875	0.94	1.535
Spectralon panel	0.67	0.67	0.67
Spectro-radiometer repeatability	0.67	0.67	0.67
Spectro-radiometer detectors	0.67	1.0	1.0
Integrating sphere repeatability	0.33	0.33	0.44
Integrating sphere uniformity	0.67	0.67	0.67
Vacuum window transmission	0.33	0.67	0.67
ALI repeatability	0.33	0.33	0.33
Total (sum in quadrature)	1.7%	1.97%	2.32%

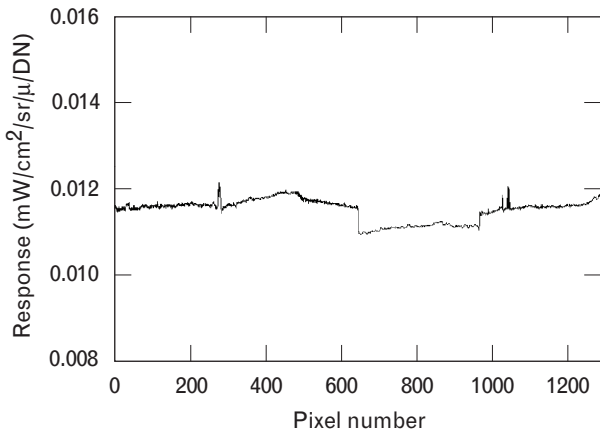


**FIGURE 8.** Radiometric calibration coefficients for band 3. The separation between the four SCA bands is evident as are several anomalous pixels. These responses are from a standard calibrated source.

#### Data Collection and Analysis

Radiometric data were collected in January 1999 in a class 1000 clean room at Lincoln Laboratory. This calibration was conducted with the ALI as a fully assembled instrument in a thermal-vacuum chamber at operational temperatures (focal plane at 220 K).

A linear function was fitted to the response of each detector to incident radiance after subtraction of the dark current. This fit may be expressed as

$$L_{\lambda}(B, I) = B_p [P_{\text{illum}, I} - P_{\text{dark}}] . \quad (2)$$

Here,  $L_{\lambda}(B, I)$  is the incident band weighted spectral radiance for band  $B$  and sphere level  $I$ ,  $B_p$  is the radiometric calibration coefficient for detector  $P$  (in units of  $\text{mW}/\text{cm}^2/\text{sr}/\mu/\text{dn}$ ),  $P_{\text{illum}, I}$  is the illuminated detector digital response for sphere level  $I$ , and  $P_{\text{dark}}$  is the dark detector digital offset.

We calculated  $L_{\lambda}(B, I)$  with the knowledge of the output radiance of the integrating sphere, the spectral response of each band, and the spectral transmission of the vacuum-tank window. This may be expressed analytically as

$$L_{\lambda}(B, I) = \frac{\int L_{\lambda}(\lambda, I) T_w(\lambda) S(b, \lambda) d\lambda}{\int S(b, \lambda) d\lambda} . \quad (3)$$

Here,  $L_{\lambda}(\lambda, I)$  is the spectro-radiometrically measured output radiance of the sphere for level  $I$ ,  $T_w$  is the spectral transmission of the vacuum-tank window,

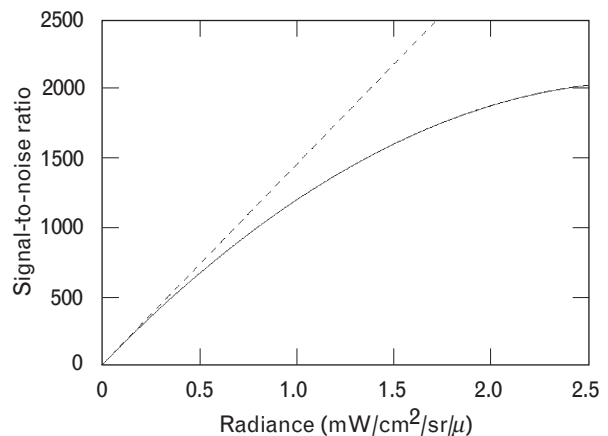
and  $S$  is the normalized spectral response for band  $B$ . The spectral response of each band used in this analysis was determined during the spectral calibration of the ALI [9].

#### Results

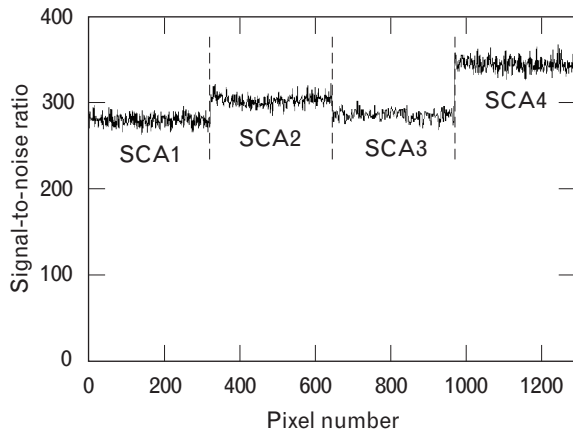
We individually derived the radiometric response of each detector of every band ( $B_p$ ) by using the method defined above. From this calibration, the response coefficient, signal-to-noise ratio, saturation radiance, and dynamic range of the ALI focal plane were determined.

Figure 8 shows the response coefficient of band 3. Detectors 0 through 319 belong to SCA 1 (outboard), detectors 320 through 639 to SCA2, detectors 640 through 959 to SCA3, and detectors 960 through 1279 to SCA 4. SCA-to-SCA and detector-to-detector variability are evident in this figure.

An individual detector's signal-to-noise ratio as a function of radiance may be derived by using the radiometric calibration in-band radiance (in units of  $\text{mW}/\text{cm}^2/\text{sr}/\mu$ ) and the detector-response and standard-deviation data. Figure 9 provides an example of the signal-to-noise ratio as a function of radiance for band 3 detector 100. Below a radiance value of 0.2, the focal-plane noise dominates and results in a linearly increasing signal-to-noise ratio. Above a radiance value of 0.2, shot noise begins to dominate and the signal-to-noise ratio begins to follow a square-root function. The dashed curve in this figure represents a linearly dependent signal-to-noise ratio.



**FIGURE 9.** Example of signal-to-noise ratio data for band 3 detector 100.



**FIGURE 10.** Signal-to-noise ratio for band 3. The distinction between the SCA bands is clear here as in Figure 8.

By fitting the data, we can calculate a predicted signal-to-noise ratio for any detector for any radiance level. Figure 10 provides the signal-to-noise ratio of band 3 for a mid-latitude summer atmosphere, solar zenith angle of  $23.5^\circ$ , 5% surface reflectance, and nadir-viewing MODTRAN (modulated resolution transmittance) model. These values are in good agreement with the signal-to-noise ratios calculated from subsystem measurements. The increase in signal-to-noise ratio levels for SCA 4 may be attributed to a lower noise for all bands of this SCA.

The saturation radiance of every detector and every band has been estimated as the product of the radiometric response coefficients and the dark-current subtracted maximum attainable value ( $dn$ ):

$$SR_p = B_p(4095 - P_{\text{dark}}) . \quad (4)$$

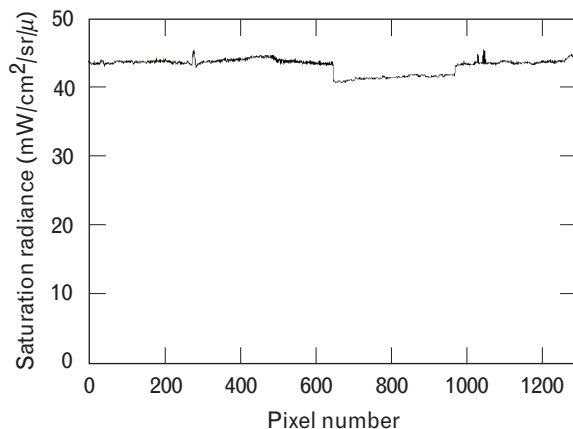


**FIGURE 11.** Saturation radiance for band 3.

Here, for detector  $P$ ,  $SR_p$  is the saturation radiance,  $P_{\text{dark}}$  is the dark offset, and  $B_p$  is the radiometric response coefficient. Adopting this method leads to the calculated saturation radiance of band 3 shown in Figure 11.

The dynamic range of the ALI focal plane has been calculated as the ratio of the maximum dark-current subtracted signal to the dark-current noise:

$$DR_p = (4095 - P_{\text{dark}}) / S_p . \quad (5)$$

Here, for detector  $P$ ,  $DR_p$  is the dynamic range,  $P_{\text{dark}}$  is the dark offset, and  $S_p$  is the noise for a dark scene (for these calculations, detector noises were assumed to be 1 dn) [11]. Figure 12 shows the calculated dynamic range of band 3 when we adopted this method.

### Summary

The results obtained in the analysis were incorporated into the calibration pipeline and were used to radiometrically calibrate initial ALI flight data. As an example of this calibration, Figure 13 depicts a band 3 image of Lincoln Laboratory before and after radiometric calibration is applied. Detector-to-detector and SCA-to-SCA variations, a result of dark-current and response coefficient variations, are clearly evident in the data prior to calibration.

### In-Flight Radiometric Calibration

After the EO-1 spacecraft was inserted into a sun-synchronous polar orbit on 21 November 2000, a rigorous in-flight radiometric calibration plan was imple-

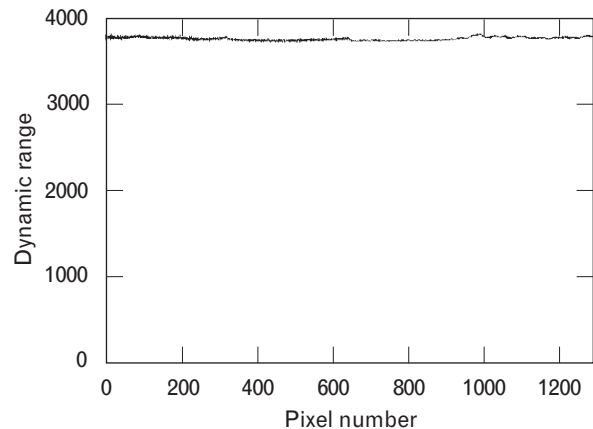


**FIGURE 12.** Dynamic range for band 3.



**FIGURE 13.** Band 3 image of Lincoln Laboratory. The image on the left is prior to radiometric calibration. The image on the right is after radiometric calibration.

mented to validate the ground characterization results and monitor the stability of the instrument.

### *Solar Calibration*

Solar calibration of the ALI is conducted approximately every fourteen days. The solar calibration procedure, illustrated in Figure 14, involves pointing the ALI at the sun with the aperture cover closed [1]. A motor-driven aperture selector in the aperture cover assembly moves an opaque slide over a row of increasingly larger slit openings and then reverses the slide motion to block all sunlight. Just prior to solar calibration, a space-grade Spectralon diffuser plate is swung over the secondary mirror by a motor-driven mechanism. The diffuser reflectively scatters the sunlight that would otherwise impinge on the secondary mirror. The scattered sunlight exposes the FPA to irradiance levels equivalent to earth-reflected sunlight for albedos ranging from 0 to 100%. The solar irradiance model used in the analysis is the MODTRAN 4.0 CHKUR model, which is currently being used for all Landsat 7 solar calibration derived gains. The radiometric calibration

and stability of the ALI are checked by comparing the expected solar radiance observed off the diffuse panel to the measured radiance in each band.\*

### *Ground Truth*

The second method of assessing the radiometric accuracy of ALI data hinges on reflectance-based ground-truth measurements [1]. The principle of this technique is to image a stable, high-altitude, flat, diffuse ground target by using the ALI while simultaneously measuring the reflective properties of the target region and local atmospheric conditions. The ground measurements can then be used to predict the top of the atmosphere radiance observed by the ALI.

Throughout the first two years of the EO-1 mission, ground-truth campaigns were conducted by sev-

---

\* On 5 July 2002, the aperture selector ceased to operate in a controllable manner, which precluded any further solar calibrations. All statistics and comparisons on stability between solar, lunar, and onboard sources were performed prior to these data. ALI is still fully operational, with calibrations and drift correction based on the lunar and onboard sources.

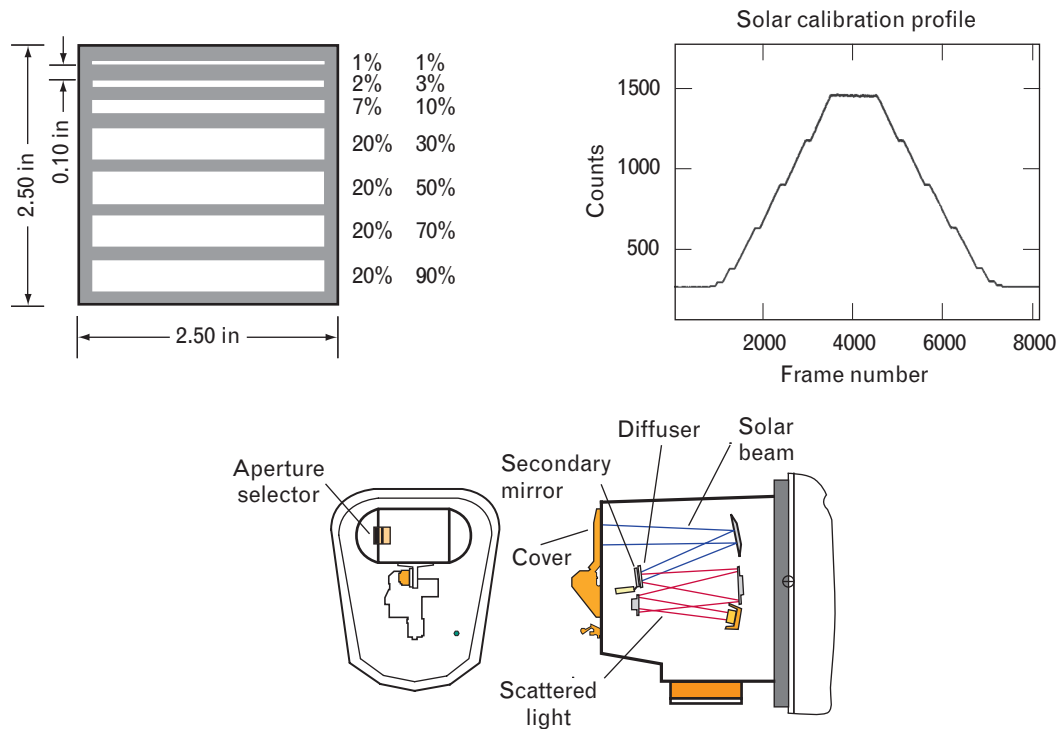


**FIGURE 14.** Illustration of the solar calibration mode and laboratory test data from a solar simulator.

eral groups, including the researchers at the University of Arizona, the University of Colorado, the Australian Commonwealth Scientific and Industrial Research Organization (CSIRO), and the NASA Jet Propulsion Laboratory. Ground-truth sites include Barreal Blanco and Arizario, Argentina; Lake Frome, Australia; and complementary sites in the western United States (Railroad Valley, Ivanpah Playa, Walnut Gulch, and White Sands).

The first step of the reflectance-based approach is to measure the reflectivity of the site to be imaged by the ALI. This task consists of obtaining several spectro-radiometric measurements of a sample portion of the site by walking a backpack-mounted sensor in a grid-like manner and averaging the results. Immediately prior to and after these measurements, spectro-radiometric measurements of a lambertian reference panel are obtained. The reflectance of the site is then obtained by ratioing the average site radiance to the average panel radiance and interpolating the result to the 1 nm level.

The second step of the reflectance-based approach is to measure the local atmospheric conditions at the

time of the EO-1 overflight. Data obtained from a multispectral solar radiometer are used as input to atmospheric modeling tools to retrieve spectral atmospheric optical depths in 1 nm intervals from 400 to 2500 nm, aerosol size distribution, and column water-to-vapor levels.

Once the surface reflectance and atmospheric conditions have been measured, a top of the atmosphere radiance is predicted at the time of the overflight. First, the solar irradiance impinging on the earth's atmosphere is determined from a solar irradiance model and sun-earth distance. Next, the effects of atmospheric scatter and absorption are accounted for by using radiative transfer modeling. The down-welling irradiance is then reflected off the site surface using the reflectivity measurements obtained previously. The atmospheric scatter and absorption effects on the upwelling radiance are accounted for by additional radiative transfer modeling, resulting in a predicted hyperspectral at-sensor radiance. Finally, the integrated product of the predicted hyperspectral radiance and ALI spectral response functions provides expected in-band radiances for the site for each spectral band. The



**FIGURE 15.** Image of the moon taken by the ALI on 7 February 2001. The circle surrounding the moon defines the regions used in the lunar irradiance calculations.

predicted in-band radiances are then compared to the observed in-band radiances, based on preflight calibration, in order to evaluate the absolute radiometry of the instrument.

#### *Lunar Calibration*

A third method used to evaluate the absolute radiometry of the ALI on-orbit is lunar calibration. This method involves observing the moon with the instrument and comparing the measured lunar spectral irradiance with a predicted lunar irradiance for the time of the observation.

Lunar observations using the ALI have been conducted near a  $7^\circ$  phase angle each month since January 2001. For each observation, the spacecraft is maneuvered to scan the moon in the in-track direction at one-eighth the nominal scan rate in order to oversample the disk. Because the moon has approximately  $\frac{1}{2}^\circ$  diameter, the entire lunar disk may be imaged on an individual SCA. As a result, four images of the moon are obtained during each lunar calibration sequence—one per sensor chip assembly.

Dark-current levels are subtracted and the image is radiometrically calibrated by using the preflight calibration coefficients to calculate the observed lunar irradiance at the time of an observation. A region of interest, narrowly circumscribing the moon (evinced

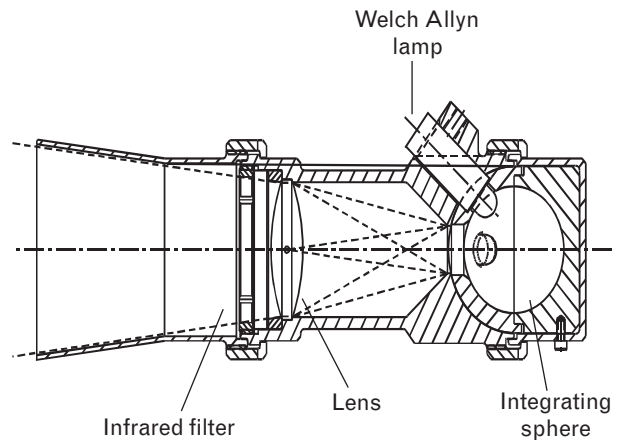


**FIGURE 16.** ALI internal reference source.

by the white circle in Figure 15), is then defined by locating the region of each column where the intensity falls to below 1% of the average lunar irradiance. The response of the instrument is then summed within the circumscribed region for each band. Next, the time, date, position of the spacecraft during the observation (geocentric coordinates), and apparent length of the lunar image (radians) are obtained from focal plane and metadata. Once the ALI data have been processed for a given observation, the information is forwarded to the USGS Robotic Lunar Observatory (ROLO) in Flagstaff, Arizona. Since 1996, ROLO has been measuring the lunar irradiance between 350 and 2500 nm as a function of phase angle as often as weather and seeing permit. Contemporaneous observations of nearby bright stars provide absolute calibration of the Observatory, as well as a measurement of atmospheric extinction. ROLO uses this database to predict lunar irradiances observed by the ALI, on the basis of the spacecraft location and phase of the moon at the time of the observation and the spectral response of the instrument for each band.

#### *Internal-Reference-Lamp Illumination*

Another source of on-orbit radiometric calibration for the ALI is an internal reference source mounted on the inside of the telescope. This source consists of three Welch Allyn 997418-7 (modified) gas-filled lamps mounted on a small (2.03 cm) diameter integrating sphere. Figure 16 shows the components of the internal reference source and Figure 17 shows its



**FIGURE 17.** Photograph of internal reference source mounted on the ALI frame.

positioning on the ALI. Light emerging from the exit slit of the sphere passes through a BK 7 lens and infrared filter, is reflected off the ALI flat folding mirror, and floods the focal plane.

The internal reference lamps are activated during

two data collection events per day, when the ALI aperture cover is closed. After an eight-second stabilization period the lamps are sequentially powered down in a staircase fashion, with two-second exposures between each step. In this manner, the focal plane will receive a daily three-point radiometric reference.

*Absolute Radiometric Response Calibration Results.* The results from an in-flight solar calibration measurement, performed on 9 February 2001 are provided in Figure 18. The measured radiances using pre-launch calibration coefficients [7] for each band have been normalized to the expected values from the Code V analysis. These data are plotted at the mean wavelength of each band. With the exception of band 1p, the solar and pre-launch calibrations agree within estimated uncertainties. The pre-launch calibration error, combined with the additional on-orbit effects of contamination and stray light, is estimated to be less than 5% for all bands. The solar calibration uncertainty is estimated to be 5% in the VNIR bands and 7% in the SWIR bands. The larger uncertainty in the SWIR bands is due to both the uncertainty in the solar irradiance models and the birefringent distribution function (BRDF) of the Spectralon. The low response in band 1p is a significant discrepancy between the measured and expected solar calibration values. A potential cause for this discrepancy is the degradation of the Spectralon diffuser, which is known to be highly susceptible to contamination. This hypothesis was ruled

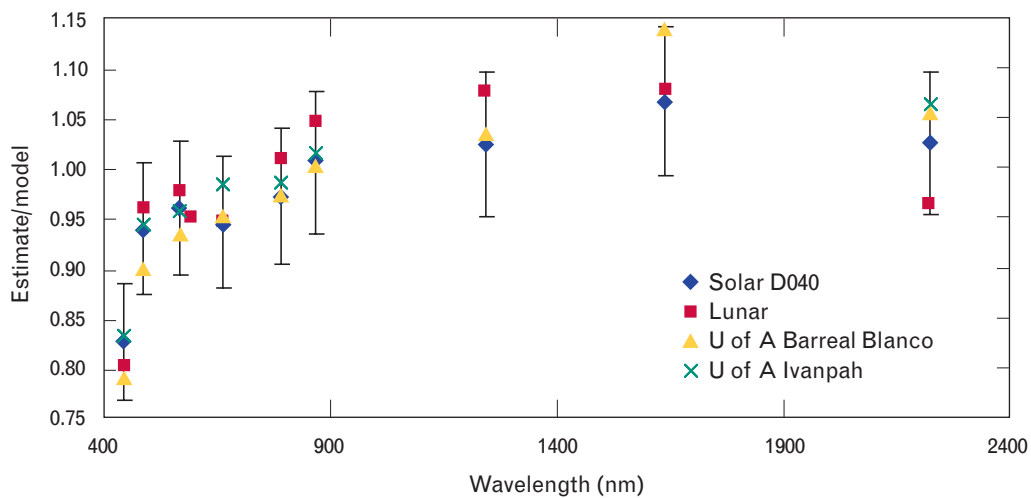


**FIGURE 18.** In-flight radiometric calibration results, normalized by the preflight calibration values. The data were compared to earth-based sensor observations.

out by comparing the solar calibration results to lunar calibration measurements and ground-truth observations.

Figure 18 overlays the results of ground truth measurements of Barreal Blanco, Argentina, and Ivanpah Playa, California, obtained by the Remote Sensing Group of the University of Arizona [3] with the solar calibration measurement presented earlier. The errors associated with the ground-truth measurements have been estimated to be  $\pm 3\%$ .

The results of a lunar irradiance comparison for measurements obtained on 7 February 2001 required a normalization of 5% to the ROLO data for all bands in order to bring the results into agreement with ALI measurements. The source of this offset is unclear at this time but the leading candidate is an uncertainty in the absolute radiometric traceability of the ROLO measurements. The absolute radiometry of the ROLO observations are currently being reviewed. However, once the 5% offset was applied, the lunar irradiance comparison result was overlaid with solar and ground-truth comparisons. Figure 18 shows this comparison and the excellent agreement between the lunar data and the other techniques, supporting the hypothesis that the radiometric response of the instrument has changed significantly for band 1p and has drooped slightly in the VNIR since preflight measurements were taken.

Initially, the internal reference source was to serve as a radiometric transfer standard between preflight and on-orbit calibrations of the ALI. However, a noticeable

increase in lamp output in the VNIR was observed immediately after launch and subsequently attributed to a loss of convective cooling of the filament in the zero-G environment. This increase in lamp output has resulted in invalidating attempts at using the reference lamps as a calibration transfer standard between preflight and flight calibration of the ALI detector arrays. However, the lamp output has been very repeatable since launch and has proven to be invaluable at monitoring the stability of the focal plane during the first two years of on-orbit operations. On the basis of these results, the internal-reference-lamp data are used solely for stability measurements.

### *Radiometric Stability*

The radiometric stability of the ALI has been tracked since launch by using the techniques outlined above. Solar calibrations occur every two weeks and began on 9 January 2001. Lunar calibrations occur monthly and began on 28 January 2001. Ground-truth measurements occur approximately every two months and began on 30 December 2000. Internal-reference-lamp measurements have been taken daily since 25 November 2000. However, only internal-reference-lamp measurements taken one day after focal-plane bake-outs are used in stability analyses.

All solar, lunar, and ground-truth calibration data presented here have had corrections applied to remove the radiometric effects of contamination on the instrument focal-plane filter surfaces. Contamination of the focal plane has been observed throughout preflight and on-orbit testing of the instrument. Fortunately, it has been demonstrated that raising the temperature of the focal plane above 250 K removes the effects of contamination beyond measurable levels. However, between bake-out periods, a build-up of contaminants on the filter surfaces has been measured. These effects have been monitored daily on-orbit by using the internal reference lamps. Figure 19 provides a history of on-orbit contamination for band 3. As is evident, a significant contamination problem existed during the first two months on-orbit. This problem was reduced below the 2% level after day 40 of the mission, finally being eliminated completely after day 400. The apparent increase in contamination near day 350 was caused by lowering the focal-plane temperature from

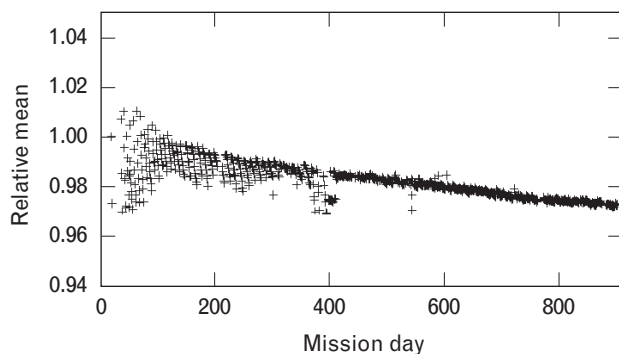


**FIGURE 19.** Band 3 contamination history. The significant contamination of the focal plane in the first two months was reduced and finally eliminated by day 400.

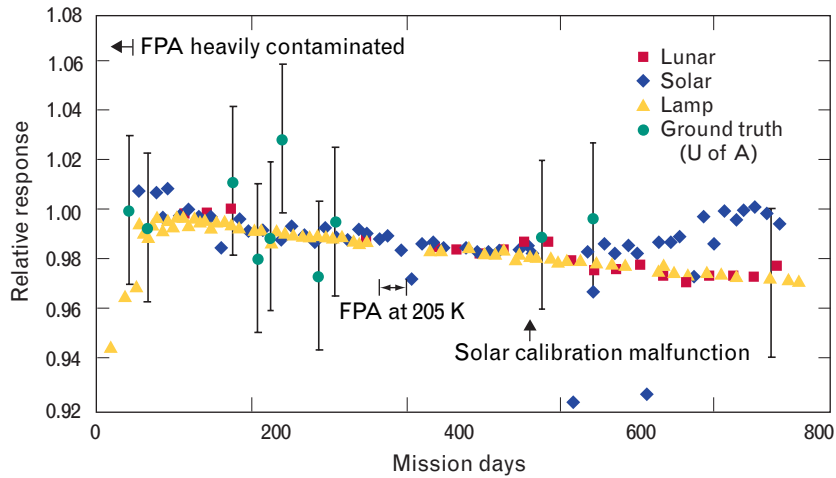


**FIGURE 20.** Trending of ALI radiometric calibration data for band 3. Two regions of the data show significant deviations that are attributed to the focal-plane array (FPA).

220 K to 205 K for thirty days as a part of an on-orbit experiment.

A contamination correction factor has been derived for each solar, lunar, and ground-truth observation by using the internal-reference-lamp data. This correction has been applied so that the intrinsic stability of the instrument may be tracked and compared by using the various calibration techniques. Because the internal-reference-lamp data selected for trending is close to periods when the instrument is baked out, the effects of contamination are minimal for these data.

*Stability Results.* Figure 20 provides the results of radiometric stability trending for SCA 1, band 3. All of the techniques described above have been overlaid in this figure. Linear fits to the data from combined internal-reference-lamp and solar calibration data are also overlaid. Table 3 lists the results of the stability trending for all spectral bands.

### Summary

An absolute radiometric calibration of the ALI was performed at Lincoln Laboratory as a part of the pre-flight calibration and characterization period. This calibration was extensively examined during the first six months that the instrument was on-orbit by using solar, lunar, and ground-truth calibration techniques. Results from each on-orbit method agree within experimental errors and indicate an 18% drop in the band 1p response of the instrument since preflight

characterization. Although we could argue the Spectralon diffuser used in the solar calibration technique could have become contaminated during ground testing or launch, radiometric calibration data that do not involve the diffuser (e.g. ground-truth and lunar observations) also observe a similar band 1p change.

**Table 3. Radiometric Stability Trending Results for First Year On Orbit**

Band	Year 1 Drift* (%)	Year 2 Drift** (%)
Panchromatic	<1.0	<1.0
1p	<1.0	<1.0
1	<1.0	<1.0
2	<1.0	-1
3	-2	-1
4	-2	-1
4p	-2	<1.0
5p	<1.0	<1.0
5	<1.0	1
7	<1.0	<1.0

\* Positive values indicate an increase in response over time, while negative values indicate a reduction in response. Values of <1.0 indicate that no drift above noise was detected.

These results exonerate the diffuser and suggest the change has occurred elsewhere in the instrument. Additionally, because the solar calibration technique does not employ the secondary mirror, this component is the only element within the optical chain that cannot be responsible for the observed change.

The on-orbit calibration data also reveal a small drooping of the other VNIR band responses (other than band 1p) towards the blue. The highest of these is a 5% decrease in radiometric response for band 1. Again, because ground-truth, lunar, and solar data reveal similar changes, only the diffuser and secondary mirror can be eliminated as sources for these changes.

*Sources of Radiometric Differences.* There are several possible sources of the radiometric discrepancies between preflight and flight measurements. The three leading candidates are (1) errors in the preflight calibration of the instrument, (2) stray light, and (3) a change in the instrument response. The preflight radiometric calibration of the ALI is based on the knowledge of the radiance emitted by a 30 inch diameter integrating sphere at several emission levels. To validate this knowledge, the NASA/Goddard-developed Landsat Transfer Radiometer (LXR) [4] was brought to Lincoln Laboratory and used to measure the sphere radiance. The LXR measurements agreed with the preflight spectro-radiometer measurements to within  $\pm 2\%$  for all eight of the LXR VNIR bands for three sphere intensity levels. This agreement includes an LXR band 10 nm wide centered at 440 nm, equivalent to band 1p of the ALI. The good agreement suggests that the preflight calibration of the ALI was well understood and measurement uncertainties cannot account for the apparent radiometric changes on-orbit in the VNIR.

Another possible source of error in ALI radiometry on-orbit is stray light. One technology being demonstrated by the ALI is large, wide field-of-view, silicon-carbide optics. Extensive preflight measurements of the BRDF for the optical elements were made. These data were used in a system-level analysis to assess the impact of stray light on flight observations. A model was developed to estimate the error in measured scene radiance as a function of the ratio of scene radiance to background radiance. This effect can be significant for dim regions of scenes with high contrast. The de-

tails of the characterization and effects of stray light on flight data are presented elsewhere [12]. However, we can state that the effects of stray light on absolute radiometric data presented here are small. Solar and internal-reference-lamp data are diffuse scenes obtained with the aperture cover closed. Ground-truth and lunar observations are bright targets in dim backgrounds, minimizing the effects of stray light from outside the target field.

The final source of observed discrepancies between preflight and flight calibration measurements is a real response change within the instrument, including a change in the reflectivity of the mirrors, the spectral band passes of the filter assemblies, or the responsivity of the detector arrays. Contamination of the top surface of the focal-plane filters has been detected since initial instrument thermal-vacuum testing. Trending of internal-reference-lamp data indicates that a gradual build-up of material occurs when the focal plane is operated below 250 K. These data also reveal that the contaminant is virtually removed by raising the temperature of the focal plane for a twenty-hour period every ten days on-orbit. This chronic problem raises suspicions relating to the apparent permanent change in instrument response since preflight calibration. However, internal-reference-lamp trending indicates the reflectivity of the flat folding mirror (M4) and the response of the focal plane have remained stable to within 1% for bands 1p, 1, 2, 5p, 5, 7, and the panchromatic band, and within 3% for bands 3, 4, and 4p since launch. Unfortunately, an observed increase in internal-reference-lamp intensity after launch prohibits us from extending focal-plane response trending from preflight calibration to on-orbit. However, trending does exist from preflight calibration at Lincoln Laboratory in December 1998 through the second spacecraft thermal-vacuum test at Goddard Space Flight Center in July 2000 (four months before launch). These data indicate M4 and the focal plane have remained stable to within 2% during ground testing. Furthermore, solar, lunar, and ground-truth data trending, which exercise other elements of the optical train, suggest the powered mirrors (M1, M2, and M3) and the solar diffuser have been stable to within 1% since the first on-orbit calibrations in late December 2000. As a result, if a response change did

**Table 4. Radiometric Correction Factors Used to Update Preflight Calibration Coefficients**

<i>Band</i>	<i>Correction Factor</i>
Panchromatic	1.05
1p	1.21
1	1.07
2	1.05
3	1.04
4	1.02
4p	0.99
5p	0.98
5	0.87
7	0.98

occur within the instrument, it must be restricted to between July 2000 and November 2000 if the change occurred on the flat folding mirror or the focal plane, or it must be restricted to between December 1998 and December 2000 if the change occurred on any of the powered mirrors.

Although the cause of the preflight-to-flight radiometric calibration discrepancy is not clearly understood, the stability of the instrument suggests a single radiometric correction to the preflight calibration coefficients for each band will provide  $\pm 5\%$  agreement between measured solar, lunar, and ground-truth data and expected values during the first two years on-orbit. Table 4 lists the radiometric correction factors derived using the above technique. We used these factors to update the preflight radiometric coefficients residing in the ALI Radiometric Calibration Pipeline.

### Stability

The ALI stability measurements using solar, lunar, ground-truth, and internal-reference-lamp data are in good agreement. All methods indicate excellent stability ( $<1\%$  per year) for bands 1p, 1, 2, 5p, 5, 7, and the panchromatic band. However, solar and lunar data indicate a 2 to 3% change per year for bands 3, 4, and 4p. Because the internal-reference-lamp data also track this trend, these changes can be isolated to the flat

folding mirror and/or focal plane. Ground-truth data also suggest these trends, but longer time lines are necessary to corroborate this result.

The band 3, 4, and 4p linear decrease in response should be monitored and correction factors applied to these data as a function of mission day number in order to preserve the absolute radiometric accuracy of ALI data for these bands.

### Acknowledgments

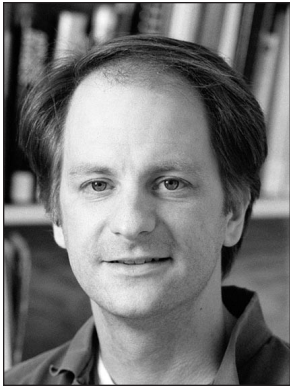
The authors wish to express their gratitude for the support provided by Danette Ryan-Howard, Alex Parker, Pat Quinn, and Eric Ringdahl during the spectral and radiometric calibration of the ALI.

---

---

## REFERENCES

1. K.J. Thome, "Absolute Radiometric Calibration of Landsat 7 ETM+ Using the Reflectance-Based Method," *Remote Sens. Environ.* 78 (1), 2001, pp. 27–38.
2. H.H. Keiffer and J.A. Anderson, "Use of the Moon for Spacecraft Calibration over 350–2500 nm," *SPIE* 3498, 1998, pp. 325–336.
3. S.F. Bigger, private communication, May 2001.
4. B. Markham, private communication, Sept. 2000.
5. J.A. Mendenhall (ed.), L.A. Bernotas, W.E. Bicknell, V.J. Cer-rati, C.J. Digenis, J.B. Evans S.E. Forman, D.R. Hearn, R.H. Hoffeld, D.E. Lencioni, D.M. Nathanson, and A.C. Parker, "Earth Observing-1 Advanced Land Imager: Instrument and Flight Operations Overview," Project Report EO-1-1, Lincoln Laboratory (23 June 2000).
6. D.E. Lencioni, C.J. Digenis, W.E. Bicknell, D.R. Hearn, and J.A. Mendenhall, "Design and Performance of the EO-1 Advanced Land Imager," *SPIE* 3870, 1999, pp. 269–280.
7. "Landsat 7 System Specification," revision K, NASA/Goddard Space Flight Center, 430-L-0002-K (July 1997).
8. J.A. Mendenhall, D.E. Lencioni, and J.B. Evans, "Earth Observing-1 Advanced Land Imager: Radiometric Response Calibration," Project Report EO-1-3, Lincoln Laboratory (29 Nov. 2000).
9. J.A. Mendenhall and D.E. Lencioni, "Earth Observing-1 Advanced Land Imager Flight Performance Assessment: Absolute Radiometry and Stability during the First Year," Project Report EO-1-10, Lincoln Laboratory (31 May 2002), DTIC #ADA-403474.
10. J.A. Mendenhall and D.P. Ryan-Howard, "Earth Observing-1 Advanced Land Imager: Spectral Response Calibration," Project Report EO-1-2, Lincoln Laboratory (20 Sept. 2000).
11. J.A. Mendenhall, "Earth Observing-1 Advanced Land Imager: Dark Current and Noise Characterization and Anomalous Detectors," Project Report EO-1-5, Lincoln Laboratory (7 May 2001), DTIC #ADA-406369.
12. J.A. Mendenhall, "Comparison of the EO-1 Advanced Land Imager Performance with the Landsat Data Continuity Mission Specification," Project Report EO-1-8, Lincoln Laboratory (4 June 2002), DTIC #ADA-403445.



**JEFFREY A. MENDENHALL** is a staff member in the Advanced Space Systems and Concepts group. He received a B.A. degree in mathematics from Saint Francis University in 1989 and a Ph.D. degree in astronomy and astrophysics from Pennsylvania State University in 1998. Immediately following graduate school he joined Lincoln Laboratory to work on the EO-1 Advanced Land Imager. His interest in this program included spectral and radiometric calibration, system engineering, and on-orbit performance assessment. Since 2001 he has tested and calibrated visible sensors that were flown on several ballistic missile defense missions. He is currently the system engineer for the Space-based Space-surveillance Technology Insertion Next Generation (SSTING) program. Jeff and his wife Linda (of the Optical Systems Engineering group), own a farm in Groton, Massachusetts, where they enjoy breeding Hanoverian horses and raising Shetland sheepdogs.



**DONALD E. LENCIONI** joined Lincoln Laboratory in 1971 after receiving a B.S. degree in physics from DePaul University and M.S. and Ph.D. degrees in physics from the University of Wisconsin–Madison. His initial research on the propagation of high-power laser beams included atmospheric breakdown, thermal blooming, and atmospheric turbulence. He became assistant leader in 1981 and then leader of the Advanced Techniques and Systems group in 1983, where he served until 1994. The focus of the group during this period was on development of passive long-wave infrared sensors. He was the associate project leader of the Optical Aircraft Measurements Program from 1983 to 1994, during which time the Cobra Eye Sensor System was developed and deployed. In 1994 he joined the Aerospace division as associate leader of the Sensor Technology and Systems group, where he initiated work on the Advanced Land Imager that was developed by Lincoln Laboratory for NASA. Currently, he is a senior staff member of the Advanced Space Systems and Concepts group, where he works on optical systems for remote sensing applications.



**JENIFER B. EVANS** is a staff member in the Space Control Systems group, where her primary responsibility is providing technical leadership in the Lincoln Near-Earth Asteroid Research (LINEAR) program. Additionally, she specializes in image processing and data analysis related to various space surveillance systems. She also provides software management and occasionally still gets a rare treat of performing actual software development. Prior to joining the Space Control Systems group, she spent six years in the Air Traffic Surveillance group, where she specialized in tracking algorithms and played a key role in the upgrade to the ASR-9 radar. She has B.S. and M.S. degrees in electrical engineering from the Ohio State University, and she joined Lincoln Laboratory in 1990. While proud of her contributions to numerous successful projects over the years, she is most proud of her accomplishments outside of the work arena, namely, her children David and Daniel, two happy, sports-loving, budding scientists. In her limited free time, she enjoys reading and attempting various outdoor sports such as skiing and golf.